JOURNAL OF COMPUTATIONAL PHYSICS 118, 242–260 (1995)

High-Order "Cyclo-Difference" Techniques: An Alternative to Finite Differences

MARK H. CARPENTER

Aerodynamic and Acoustic Methods Branch, NASA Langley Research Center, Hampton, Virginia 23681

AND

JOHN OTTO

Multidisciplinary Design Optimization Branch, NASA Langley Research Center, Hampton, Virginia 23681

Received March 26, 1993; revised August 10, 1994

The summation-by-parts energy norm is used to establish a new class of high-order finite-difference techniques referred to here as "cyclo-difference" techniques. These techniques are constructed cyclically from stable subelements and require no special numerical procedures near the boundaries; when coupled with the simultaneous approximation term (SAT) boundary treatment, they are time asymptotically stable for an arbitrary hyperbolic system. These techniques are similar to spectral multi-domain techniques and are ideally suited for parallel implementation, but they do not require special collocation points. The principal focus of this work is on methods of sixth-order formal accuracy or less; however, these methods could be extended in principle to any arbitrary order of accuracy.

INTRODUCTION

A great deal of effort has recently been placed on high-order finite-difference techniques (both central and upwind) for direct numerical simulations. A significant issue high-order finite-difference schemes must address is determining stable "near boundary" procedures that retain the formal accuracy of the underlying method. To retain the Nth-order formal accuracy of the interior scheme for an arbitrary hyperbolic equation, the numerical boundaries must be closed with an accuracy of no less than $(N-1)$th order [1]. Many high-order closures (greater than fifth-order accuracy) cause numerical instability and cannot be used (e.g., [2]). Recently, a precise means of determining boundary closures that maintain both stability and accuracy has been developed based on the summation-by-parts energy norm. (See Refs. [3–5].) A numerical discretization that satisfies specific criteria on the discretization matrix A^* automatically satisfies a discrete energy norm. Central-difference schemes automatically satisfy these properties in their interior. The task is, therefore, to find high-order closure techniques at the boundaries that maintain the specific form of the matrix A^*. This is a daunting task, but it can be accomplished [2–5].

One advantage spectral techniques have that conventional finite difference ones do not is that numerical boundary procedures are not required. The global nature of the method relies on a specific stencil at each point. Each individual point may be unstable, but the scheme as a whole is stable and accurate. This notion motivates us to develop a new class of finite-difference schemes. Like central-difference and spectral techniques, they are not biased in the direction of a physical eigenvalue and, therefore, do not require eigenvalue decomposition when used for general hyperbolic equations. Unlike central-difference techniques, each point has its own specific stencil. Although individual stencils may appear to be unstable locally, the global method is stable and accurate. Taylor series analysis guarantees that each point has a local order property. The use of a specific energy norm to derive the stencils guarantees that the resulting global scheme is stable.

Implementation on parallel machines, of high-order finite-difference techniques and single-domain spectral techniques, can be complicated. For conventional finite-difference techniques (central or upwind difference) as the order of accuracy increases the stencil width also increases. This results in increased overhead in communicating between processors. Spectral element (or multi-domain) techniques are both efficient and accurate methods for implementation on parallel machines [6]. The problem is divided into several domains and each domain is assigned to a processor. Only one point of the stencil coexists on multiple processors in spectral element techniques. Information transfer between processors is kept to a minimum under these circumstances.

Cyclo-difference techniques are a combination of high-order finite-difference techniques and spectral element techniques. They rely on an existing energy-norm proof to establish their stability for the hyperbolic system and require no special boundary closure stencils. These techniques can easily be split on multi-processor environments. This flexibility results because the discretizations are composed of many subelements that each

0021-9991/95 $6.00

satisfy an order and stability property. The subelements are then patched together recursively such that the resulting scheme retains the same stability properties. For parallel implementation, they can easily be broken at the patch location, which results in a minimum of communication for an arbitrarily high-order scheme.

SUMMATION-BY-PARTS ENERGY NORM

Stability of Continuous System

As shown in Ref. [5], the summation-by-parts energy norm mimics, at the semidiscrete level, the continuous behavior of the principle of the conservation of energy. Because the entire foundation of the cyclo-difference methodology is based on this norm, a complete derivation of the conservation of energy principle in the continuous and the discrete case is presented. The model problem is the hyperbolic equation defined by

$$\frac{\partial U}{\partial t} + \frac{\partial U}{\partial x} = 0, \quad 0 \le x \le 1, t \ge 0, \tag{1}$$

$$U(0, t) = f(t), \quad t \ge 0, \tag{2}$$

$$U(x, 0) = \psi(x), \quad 0 \le x \le 1, \tag{3}$$

We begin by defining an energy as $E(t) = U^2$, $t > 0$. If the energy is differentiated with respect to time and the values of U_t from Eq. (1) are substituted, then integration over the domain yields

$$E_t(t) = \int_0^1 \left[-\frac{\partial(U^2)}{\partial x} \right] dx, \quad t \ge 0. \tag{4}$$

The definite integral in Eq. (4) is performed to yield

$$E_t(t) = -[U^2(1, t) - U^2(0, t)] \tag{5}$$

and the boundary conditions are substituted from Eq. (2) to yield

$$E_t(t) = -[U^2(1, t) - f^2(t)]. \tag{6}$$

If certain properties on the boundary condition $f(t)$ are assumed, the equation energy decreases for all time. For example, if $f(t) = 0$, then the system energy decreases uniformly as energy flows out of the domain.

Stability of Discrete System

Discrete spatial operators that satisfy very specific properties are shown to be stable in a manner analogous to that used in the previous proof of stability. These operators satisfy the summation-by-parts energy norm. For example, given the scalar hyperbolic equation $U_t + U_x = 0$, a general semidiscretization can be written as $U_t + A^*U = 0$, where A^* is the spatial discretization matrix that is presumably consistent to some order. This matrix A^* can, in general, be decomposed into the form

$$A^* = P^{-1}Q. \tag{7}$$

This decomposition is in general not unique. If a decomposition can be found:

1. Symmetric P: $(P = P^T)$ $(p_{i,j} = p_{j,i})$
2. Positive definite P: $(W^TPW > 0)$
3. Nearly skew-symmetric Q: $(q_{i,j} + q_{j,i} = 2\delta_{i,1}\delta_{1,j}q_{1,1} + 2\delta_{i,N}\delta_{N,j}q_{N,N})$
4. $q_{N,N} = -q_{1,1} = \frac{1}{2}$

then the discretization matrix A^* automatically satisfies the summation-by-parts energy norm. (See Ref. [5].)

To illustrate that this stability property results directly from the form of the matrices P and Q, a proof is presented for the semidiscrete form defined by Eqs. (1) and (2). Note that the spatial discretization operator can be written in the form

$$PU_x = QU; \quad U_x = P^{-1}QU, \tag{8}$$

where P^{-1} exists and U is the vector of discrete values $(U_1, U_2, U_3, \ldots U_{N-2}, U_{N-1}, U_N)^T$. The semidiscrete version of Eq. (1) becomes

$$P\frac{\partial U}{\partial t} + QU = 0, \quad t \ge 0. \tag{9}$$

We define the discrete energy as

$$E(t) = (U^TPU), \quad t \ge 0, \tag{10}$$

where P must be positive definite to ensure that $E(t)$ is a strictly positive number. Equation (10) is differentiated with respect to time to yield the expression

$$E_t(t) = \left[\frac{\partial U^T}{\partial t} PU + U^TP\frac{\partial U}{\partial t} \right], \quad t \ge 0. \tag{11}$$

Because P is symmetric $(P = P^T)$, Eq. (11) becomes

$$E_t(t) = 2\left[U^TP\frac{\partial U}{\partial t} \right], \quad t \ge 0. \tag{12}$$

The semidiscrete expression (Eq. (9)) is substituted into Eq. (12) to yield

$$E_t(t) = 2[-U^TQU], \quad t \ge 0. \tag{13}$$

By using the matrix Q and the relationship between the values $q_{0,0}$ and $q_{N,N}$, one obtains an energy of the form

$$E_t(t) = -2q_{N,N}[U_N^2 - U_0^2]. \tag{14}$$

The boundary condition defined in Eq. (2) is substituted to yield

$$E_t(t) = -2q_{N,N}[U_N^2 - f^2(t)]. \tag{15}$$

Note that the time rate of change of the discrete energy defined in Eq. (15) is identical in form (to within a positive constant) to that of the continuous case equation (5).

CYCLO-DIFFERENCING

Conventional central- and upwind-difference techniques use one stencil for the inner portion of the spatial domain and auxiliary formulas at the boundaries such that the resulting scheme is stable. Spectral element techniques use orthogonal basis functions to define local elements and then connect them with various methods that range from spectral patching to flux balances [7]. The simplicity and stability of the cyclo-differencing relies on a very specific property of the summation-by-parts energy norm. Assume for a particular set of discrete points x_j, $j = 1, N$, that a stable discretization has been isolated that satisfies all criteria of the summation-by-parts energy norm. The resulting semidiscretization written in matrix form is $P\mathbf{U}_t = Q\mathbf{U}$, where

$$P = \begin{bmatrix} p_{1,1} & p_{1,2} & \cdots & p_{1,N-1} & p_{1,N} \\ p_{1,2} & p_{2,2} & \cdots & p_{2,N-1} & p_{2,N} \\ \cdot & \cdot & & \cdot & \cdot \\ \cdot & \cdot & & \cdot & \cdot \\ \cdot & \cdot & & \cdot & \cdot \\ p_{1,N-1} & p_{1,N-2} & \cdots & p_{N-1,N-1} & p_{N-1,N} \\ p_{1,N} & p_{2,N} & \cdots & p_{N-1,N} & p_{N,N} \end{bmatrix};$$

$$\mathbf{U}_t = \begin{bmatrix} \partial U_1/\partial t \\ \partial U_2/\partial t \\ \cdot \\ \cdot \\ \partial U_{N-1}/\partial t \\ \partial U_N/\partial t \end{bmatrix};$$

$$Q = \frac{1}{\Delta}\begin{bmatrix} -q_{N,N} & q_{1,2} & \cdots & q_{1,N-1} & q_{1,N} \\ -q_{1,2} & 0 & \cdots & q_{2,N-1} & q_{2,N} \\ \cdot & \cdot & \cdot & \cdot & \cdot \\ \cdot & \cdot & \cdot & \cdot & \cdot \\ \cdot & \cdot & \cdot & \cdot & \cdot \\ -q_{1,N-1} & -q_{1,N-2} & \cdots & 0 & q_{N-1,N} \\ -q_{1,N} & -q_{2,N} & \cdots & -q_{N-1,N} & q_{N,N} \end{bmatrix};$$

$$\mathbf{U} = \begin{bmatrix} U_1 \\ U_2 \\ \cdot \\ \cdot \\ U_{N-1} \\ U_N \end{bmatrix}.$$

Note that P is symmetric (and positive definite) and Q is skew symmetric, except for the elements $q_{1,1}$ and $q_{N,N}$, where $q_{1,1} = -q_{N,N}$. Also note that the grid-spacing Δ has been factored out of the matrix Q. No attempt has been made to specify the value of the constant N. A cyclo-difference scheme is constructed by recursively patching the stable base schemes together, which is illustrated by the following example. Assume that the discretization involved $2N - 1$ uniformly distributed points instead of N points. We can use the properties of the matrices P and Q (of dimension N) to define a discretization over the $2N - 1$ points that satisfies all criteria of the summation-by-parts energy norm and is therefore stable for any system of hyperbolic equations. We define this new semidiscretization on the equation $U_t + U_x = 0$ as $\hat{P}\hat{\mathbf{U}}_t = \hat{Q}\hat{\mathbf{U}}$ and construct it as

$$\hat{P} = \begin{bmatrix} p_{1,1} & p_{1,2} & \cdots & p_{1,N-1} & p_{1,N} & 0 & \cdots & 0 & 0 \\ p_{1,2} & p_{2,2} & \cdots & p_{2,N-1} & p_{2,N} & 0 & \cdots & 0 & 0 \\ \cdot & \cdot & & \cdot & \cdot & 0 & \cdots & 0 & 0 \\ \cdot & \cdot & & \cdot & \cdot & 0 & \cdots & 0 & 0 \\ \cdot & \cdot & & \cdot & \cdot & 0 & \cdots & 0 & 0 \\ p_{1,N-1} & p_{2,N-1} & \cdots & p_{N-1,N-1} & p_{N-1,N} & 0 & \cdots & 0 & 0 \\ p_{1,N} & p_{2,N} & \cdots & p_{N-1,N} & p_{N,N} + p_{1,1} & p_{1,2} & \cdots & p_{1,N-1} & p_{1,N} \\ 0 & 0 & \cdots & 0 & p_{1,2} & p_{2,2} & \cdots & p_{2,N-1} & p_{2,N} \\ 0 & 0 & \cdots & 0 & \cdot & \cdot & & \cdot & \cdot \\ 0 & 0 & \cdots & 0 & \cdot & \cdot & & \cdot & \cdot \\ 0 & 0 & \cdots & 0 & \cdot & \cdot & & \cdot & \cdot \\ 0 & 0 & \cdots & 0 & p_{1,N-1} & p_{2,N-1} & \cdots & p_{N-1,N-1} & p_{N-1,N} \\ 0 & 0 & \cdots & 0 & p_{1,N} & p_{2,N} & \cdots & p_{N-1,N} & p_{N,N} \end{bmatrix};$$

$$\hat{Q} = \frac{1}{\Delta}\begin{bmatrix}
-q_{N,N} & q_{1,2} & \cdots & q_{1,N-1} & q_{1,N} & 0 & \cdots & 0 & 0 \\
-q_{1,2} & 0 & \cdots & q_{2,N-1} & q_{2,N} & 0 & \cdots & 0 & 0 \\
. & . & & . & . & 0 & \cdots & 0 & 0 \\
. & . & & . & . & 0 & \cdots & 0 & 0 \\
. & . & & . & . & 0 & \cdots & 0 & 0 \\
-q_{1,N-1} & -q_{2,N-1} & \cdots & 0 & q_{N-1,N} & 0 & \cdots & 0 & 0 \\
-q_{1,N} & -q_{2,N} & \cdots & -q_{N-1,N} & 0 & q_{1,2} & \cdots & q_{1,N-1} & q_{1,N} \\
0 & 0 & \cdots & 0 & -q_{1,2} & 0 & \cdots & q_{2,N-1} & q_{2,N} \\
0 & 0 & \cdots & 0 & . & . & & . & . \\
0 & 0 & \cdots & 0 & . & . & & . & . \\
0 & 0 & \cdots & 0 & . & . & & . & . \\
0 & 0 & \cdots & 0 & -q_{1,N-1} & -q_{2,N-1} & \cdots & 0 & q_{N-1,N} \\
0 & 0 & \cdots & 0 & -q_{1,N} & -q_{2,N} & \cdots & -q_{N-1,N} & q_{N,N}
\end{bmatrix},$$

where $\hat{\mathbf{U}} = [U_1, U_2, \ldots U_{N-1}, U_N, U_{N+1}, \ldots U_{2N-2}, U_{2N-1}]^T$. Note that the $\hat{q}_{N,N}$ element is precisely zero because the contributions from $q_{1,1}$ and $q_{N,N}$ have equal magnitudes but opposite signs. These new matrices $\hat{P}$ and $\hat{Q}$ satisfy the summation-by-parts energy norm for precisely the same reasons as the original matrices P and Q. If the matrices are assembled in this manner, then the matrix $\hat{P}$ is symmetric and the matrix $\hat{Q}$ is skew symmetric except for the (1, 1) and $(2N-1, 2N-1)$ elements; these coefficients are again equal in magnitude but opposite in sign. Because the matrix $\hat{P}$ can be decomposed into the summation of two matrices $\hat{P}_1$ and $\hat{P}_2$, each of which is positive definite (one, but not both, could be positive semidefinite), the resulting matrix $\hat{P}$ is positive definite. The new scheme is therefore stable because the summation-by-parts energy norm is satisfied. In practice, the scheme would be implemented as $\hat{U}_t = \hat{P}^{-1}\hat{Q}\hat{\mathbf{U}}$. The inversion of the matrix $\hat{P}$ could in general be quite complicated.

In short-hand notation, the new matrices $\hat{P}$ and $\hat{Q}$ can be written in terms of the original matrices P and Q as

$$\hat{P} = \begin{bmatrix} P & 0 \\ 0 & P \end{bmatrix}; \quad \hat{Q} = \frac{1}{\Delta}\begin{bmatrix} Q & 0 \\ 0 & Q \end{bmatrix}.$$

This nomenclature is not precisely correct because the new matrix $\hat{P}$ is $(2N-1 \times 2N-1)$, and the original P is $(N \times N)$. More precisely, the last row of the first matrix P and the first row of the second matrix P lie on the same row of the new matrix $\hat{P}$, with the inevitable intersection of matrices at the point $\hat{p}_{N,N}$. For the purposes of this work, this nomenclature will not cause any ambiguities.

Thus far in the derivation, we have assumed that the grid spacing in the first subdomain was the same as that in the second domain. In general, this assumption is not necessary, which we will demonstrate. Suppose that the first interval is discretized with a grid spacing Δ_1 and the second with a spacing Δ_2. The resulting semidiscretizations would be $P\mathbf{U}_t = (1/\Delta_1)\,Q\mathbf{U}$ and $P\mathbf{U}_t = (1/\Delta_2)\,Q\mathbf{U}$, respectively. Each respective discretization is multiplied by the appropriate grid spacing to yield $\Delta_1 P\mathbf{U}_t = Q\mathbf{U}$ and $\Delta_2 P\mathbf{U}_t = Q\mathbf{U}$, respectively. The two subintervals are combined into one to yield the matrices $\hat{P}$ and $\hat{Q}$ of the form

$$\hat{P} = \begin{bmatrix} \Delta_1 P & 0 \\ 0 & \Delta_2 P \end{bmatrix}; \quad \hat{Q} = \begin{bmatrix} Q & 0 \\ 0 & Q \end{bmatrix}.$$

The stability of the resulting scheme is guaranteed by the summation-by-parts energy norm for any arbitrary spacing discontinuity. In practice, the scheme would be implemented as $\hat{U}_t = \hat{P}^{-1}\hat{Q}\mathbf{U}$. The inversion of the matrix $\hat{P}$ could in general be quite complicated. All information that pertains to the discontinuity in spacing is incorporated into the $\hat{P}$ matrix.

This procedure of appending new subintervals onto an already existing method can be repeated recursively as many times as desired. In fact, even two dissimilar methods (each of which satisfies the summation-by-parts energy norm) can be appended to one another on any arbitrary grid-spacing interval. One constraint which the resulting cyclo-difference schemes must satisfy, is that the total number of grid points must be of the form $N_t = M(N-1) + 1$, where N_t is the total number of points and M is the number of subintervals that are used. The procedure for grid refinement, therefore, involves increasing the number of subintervals M in the solution. (Or as in finite-elements, one could choose higher order elements and the same number of total grid points.)

Boundary Conditions

We begin by distinguishing between the numerical procedures which are motivated by accuracy and stability concerns, from those required to satisfy the physical boundary condition of the governing differential equation. Unlike conventional finite-difference schemes, cyclo-difference schemes of any order, only consider the physical boundary conditions necessary to satisfy the partial differential equation; there are no auxiliary stencils near the boundaries which are motivated by accuracy or global stability.

Consider, for example, the fourth-order explicit finite-difference scheme on $N + 1$ uniform grids $0 \leq j \leq N$. The stencil width is five points, centered about the point j for $2 \leq j \leq N - 1$. At grid points 0 and 1 (as well as points $N - 1$ and N) auxiliary formula must be used, because the interior five point stencil involves information from outside the domain. To retain the fourth-order formal accuracy of the interior scheme for an arbitrary hyperbolic equation, the numerical boundaries must be closed with an accuracy of no less than third-order [1]. In this case, stable third-order closures are readily available. In general, however, the complexity of stable and accurate numerical boundary procedures increases with the order of the interior scheme. For schemes of sixth-order and higher, satisfying the stability and accuracy constraints near the boundaries becomes a major obstacle in using high-order finite difference schemes [2].

Cyclo-difference schemes do not suffer from this problem. Each element is stable and accurate, and is well-defined throughout their domain. The boundary points 0 and N are simply the first and last points, respectively, in the domain of the fundamental element. The only constraint (as mentioned earlier) is that the total number of points be a multiple of the element size plus one. Clearly, this argument holds for any size element, or order of accuracy.

The imposition of the physical boundary condition is a delicate issue if stability and accuracy are both to be preserved. The cyclo-difference schemes satisfy a semi-discrete summation-by-parts energy norm and have the special property that the matrix P is a restricted full norm (see Strand [4]). It was shown in Ref. [5] that schemes satisfying the semi-discrete summation-by-parts energy norm are stable for any constant coefficient hyperbolic system, if the physical boundary conditions are implemented by a simultaneous-approximation-term (SAT) treatment. The SAT procedure simultaneously approximates (while preserving the order property of the overall scheme) the differential equation and the physical boundary condition at the boundary of the domain. Because the cyclo-difference schemes have a restricted full norm P, they are automatically stable for the semi-discrete scalar hyperbolic equation, even without the SAT boundary treatment. Details on these and other stability related issues can be found elsewhere [5] and are not given in detail in this work.

To guarantee the accuracy of the full-discrete equations, a special procedure was devised in reference [12] for implementing the physical boundary conditions. (True for any spatial operator, not just cyclo-difference spatial operators.) If an ordinary differential equation (ODE) is derived on the boundary by differentiating the boundary condition with respect to time and then is solved with the same time advancement scheme used in the interior portion of the domain, then accuracy can be proven for the constant coefficient hyperbolic system [12].

HIGH-ORDER CYCLO-DIFFERENCE SCHEMES

Second Order

We now present a variety of cyclo-difference schemes of various order and width. In this work, we will concentrate on schemes with uniform grid spacing within each subelement (but not necessarily the same from element to element). The first scheme of practical interest is the second-order scheme defined on a subelement of three grid points. The scheme represents the optimal second-order scheme on three uniformly spaced grid points and, in matrix notation, is given by

$$A^* = \begin{bmatrix} \frac{-3}{2} & 2 & \frac{-1}{2} \\ \frac{-1}{2} & 0 & \frac{1}{2} \\ \frac{1}{2} & -2 & \frac{3}{2} \end{bmatrix}.$$

It is readily shown that $A^* = P^{-1}Q$, where

$$P = \begin{bmatrix} \frac{1}{4} & 0 & 0 \\ 0 & 1 & 0 \\ 0 & 0 & \frac{1}{4} \end{bmatrix}; \quad Q = \begin{bmatrix} \frac{-3}{8} & \frac{1}{2} & \frac{-1}{8} \\ \frac{-1}{2} & 0 & \frac{1}{2} \\ \frac{1}{8} & \frac{-1}{2} & \frac{3}{8} \end{bmatrix}.$$

This scheme is extended to five grid points to yield $\hat{P}$ and $\hat{Q}$ of the form

$$\hat{P} = \begin{bmatrix} \frac{1}{4} & 0 & 0 & 0 & 0 \\ 0 & 1 & 0 & 0 & 0 \\ 0 & 0 & \frac{1}{2} & 0 & 0 \\ 0 & 0 & 0 & 1 & 0 \\ 0 & 0 & 0 & 0 & \frac{1}{4} \end{bmatrix}; \quad \hat{Q} = \begin{bmatrix} \frac{-3}{8} & \frac{1}{2} & \frac{-1}{8} & 0 & 0 \\ \frac{-1}{2} & 0 & \frac{1}{2} & 0 & 0 \\ \frac{1}{8} & \frac{-1}{2} & 0 & \frac{1}{2} & \frac{-1}{8} \\ 0 & 0 & \frac{-1}{2} & 0 & \frac{1}{2} \\ 0 & 0 & \frac{1}{8} & \frac{-1}{2} & \frac{3}{8} \end{bmatrix}.$$

Because of the diagonal nature of the matrix $\hat{P}$, $\hat{P}^{-1}$ is easily found; the resulting numerical scheme is

$$\hat{A}^* = \begin{bmatrix} \frac{-3}{2} & 2 & \frac{-1}{2} & 0 & 0 \\ \frac{-1}{2} & 0 & \frac{1}{2} & 0 & 0 \\ \frac{1}{4} & -1 & 0 & 1 & \frac{-1}{4} \\ 0 & 0 & \frac{-1}{2} & 0 & \frac{1}{2} \\ 0 & 0 & \frac{1}{2} & -2 & \frac{3}{2} \end{bmatrix}.$$

The procedure is extended recursively to an arbitrary number of subelements to yield a cyclo-difference scheme of the form

$$\hat{A}^* = \begin{bmatrix} \frac{-3}{2} & 2 & \frac{-1}{2} & 0 & 0 & 0 & 0 & 0 & 0 & 0 & 0 & 0 & 0 \\ \frac{-1}{2} & 0 & \frac{1}{2} & 0 & 0 & 0 & 0 & 0 & 0 & 0 & 0 & 0 & 0 \\ \frac{1}{4} & -1 & 0 & 1 & \frac{-1}{4} & 0 & 0 & 0 & 0 & 0 & 0 & 0 & 0 \\ 0 & 0 & \frac{-1}{2} & 0 & \frac{1}{2} & 0 & 0 & 0 & 0 & 0 & 0 & 0 & 0 \\ 0 & 0 & \frac{1}{4} & -1 & 0 & 1 & \frac{-1}{4} & 0 & 0 & 0 & 0 & 0 & 0 \\ 0 & 0 & 0 & 0 & . & . & . & 0 & 0 & 0 & 0 & 0 & 0 \\ 0 & 0 & 0 & 0 & 0 & . & . & . & 0 & 0 & 0 & 0 & 0 \\ 0 & 0 & 0 & 0 & 0 & 0 & . & . & . & 0 & 0 & 0 & 0 \\ 0 & 0 & 0 & 0 & 0 & 0 & \frac{1}{4} & -1 & 0 & 1 & \frac{-1}{4} & 0 & 0 \\ 0 & 0 & 0 & 0 & 0 & 0 & 0 & 0 & \frac{-1}{2} & 0 & \frac{1}{2} & 0 & 0 \\ 0 & 0 & 0 & 0 & 0 & 0 & 0 & 0 & \frac{1}{4} & -1 & 0 & 1 & \frac{-1}{4} \\ 0 & 0 & 0 & 0 & 0 & 0 & 0 & 0 & 0 & 0 & \frac{-1}{2} & 0 & \frac{1}{2} \\ 0 & 0 & 0 & 0 & 0 & 0 & 0 & 0 & 0 & 0 & \frac{1}{2} & -2 & \frac{3}{2} \end{bmatrix}.$$

This scheme is uniformly second-order accurate and satisfies the summation-by-parts energy norm. In addition, the scheme does not rely on auxiliary stencils at the boundaries. The operation count is $\frac{3}{2}$ of the count for the conventional second-order scheme and, as will be shown later, behaves noticeably different.

In general, a closed-form expression for $\hat{A}^*$ will not be available because the inverse of $\hat{P}$ will not be known analytically. Therefore, a banded or an "LU" solver of width $2N - 1$ (the number of points in each subelement) can be used on the matrix $\hat{P}$ to efficiently invert the matrix. Although these solvers are efficient in comparison with full solvers, they cannot compete with explicit schemes in which no numerical inversion of the matrix $\hat{P}$ must be performed. The previous example demonstrates that methods with a diagonal matrix P can be immediately inverted. By only concerning ourselves with those numerical methods that possess this property, we are being overly restrictive. In general, if P has a first and a last row that consists entirely of zeroes, except for the diagonal element, then each subelement of the resulting matrix $\hat{P}$ decouples and the inverse can be performed analytically. The resulting scheme has an explicit, not implicit, operation count and can compete with conventional finite-difference schemes of comparable spatial accuracy.

Third Order

A uniformly third-order scheme can be generated with a minimum of four discrete points. The discretization matrix A^*, which is third order and occupies four points, can be represented as

$$A^* = \begin{bmatrix} -\frac{11}{6} & 3 & -\frac{3}{2} & \frac{1}{3} \\ -\frac{1}{3} & -\frac{1}{2} & 1 & -\frac{1}{6} \\ \frac{1}{6} & -1 & \frac{1}{2} & \frac{1}{3} \\ -\frac{1}{3} & \frac{3}{2} & -3 & \frac{11}{6} \end{bmatrix}.$$

If A^* is decomposed into $P^{-1}Q$, the resulting relationships for P and Q are

$$P = \begin{bmatrix} r3 & \frac{360\,r3 - 11\,r2 + 21\,r1}{312} & \frac{-(54\,r3 - r2 + 9\,r1)}{78} & \frac{120\,r3 + 5\,r2 + 33\,r1}{312} \\ \frac{360\,r3 - 11\,r2 + 21\,r1}{312} & \frac{207\,r3 + 7\,r2 + 15\,r1}{39} & \frac{-(72\,r3 + 55\,r2 + 51\,r1)}{312} & \frac{-(54\,r3 - r2 + 9\,r1)}{78} \\ \frac{-(54\,r3 - r2 + 9\,r1)}{78} & \frac{-(72\,r3 + 55\,r2 + 51\,r1)}{312} & \frac{207\,r3 + 7\,r2 + 15\,r1}{39} & \frac{360\,r3 - 11\,r2 + 21\,r1}{312} \\ \frac{120\,r3 + 5\,r2 + 33\,r1}{312} & \frac{-(54\,r3 - r2 + 9\,r1)}{78} & \frac{360\,r3 - 11\,r2 + 21\,r1}{312} & r3 \end{bmatrix};$$

$$Q = \begin{bmatrix} \frac{-(288\,r3 - r2 + 9\,r1)}{117} & \frac{384\,r3 + 3\,r2 + 25\,r1}{104} & \frac{-(24\,r3 - r2 + 4\,r1)}{13} & \frac{576\,r3 + 37\,r2 + 135\,r1}{936} \\ \frac{-(384\,r3 + 3\,r2 + 25\,r1}{104} & 0 & \frac{576\,r3 + 11\,r2 + 57\,r1}{104} & \frac{-(24\,r3 + r2 + 4\,r1)}{13} \\ \frac{24\,r3 + r2 + 4\,r1)}{13} & \frac{-(576\,r3 + 11\,r2 + 57\,r1)}{104} & 0 & \frac{384\,r3 + 3\,r2 + 25\,r1}{104} \\ \frac{-(576\,r3 + 37\,r2 + 135\,r1)}{936} & \frac{24\,r3 + r2 + 4\,r1}{13} & \frac{-(384\,r3 + 3\,r2 + 25\,r1}{104} & \frac{288\,r3 - r2 + 9\,r1}{117} \end{bmatrix};$$

The final criteria to be met is that the matrix P must be positive definite. Even if this scheme was stable for arbitrary $r1$, $r2$, and $r3$, the amount of work necessary to invert the matrix P would make the scheme prohibitively expensive. Therefore, the free parameters are used to decrease the bandwidth of the matrix P. If we set $r3 = 1$, $r2 = 9\,r3$, and $r1 = -5\,r3$, then P and Q results are

$$P = \begin{bmatrix} 1 & \frac{1}{2} & 0 & 0 \\ \frac{1}{2} & 5 & -1 & 0 \\ 0 & -1 & 5 & \frac{1}{2} \\ 0 & 0 & \frac{1}{2} & 1 \end{bmatrix}; \quad Q = \begin{bmatrix} -2 & \frac{11}{4} & -1 & \frac{1}{4} \\ \frac{-11}{4} & 0 & \frac{15}{4} & -1 \\ 1 & \frac{-15}{4} & 0 & \frac{11}{4} \\ \frac{-1}{4} & 1 & \frac{-11}{4} & 2 \end{bmatrix}.$$

With Gershgorin's theorem (diagonal dominance) the matrix P is shown to be positive definite. The original matrix satisfies the summation-by-parts energy norm and is stable for the hyperbolic system. Unfortunately, not enough free parameters exist in the decomposition to make P diagonal. The work involved in using a cyclo-difference scheme generated from P and Q would be seven multiplications and additions per node: four from the Q matrix and three from the inversion of the tridiagonal matrix $\hat{P}$. An operation count this high would not make the resulting scheme competitive with other third or higher order schemes.

To obtain high-order schemes in which P can be diagonalized, or at least decoupled from the other subelements, nonoptimal schemes must be used. Consider, for example, the family of uniformly third-order schemes that can be defined on five uniform points. Because each point allows a new degree of freedom, a wide variety of different schemes can be developed. Assuming that the following constraints are imposed: (1) uniform third-order accuracy exists from five points, (2) a P and Q exist that satisfy the summation-by-parts energy norm, and (3) a matrix P exists that has a first and last row composed entirely of zeros except the diagonal element. Matrices P and Q result in the forms

$$P = \begin{bmatrix} -\frac{67\xi-3}{1552} & 0 & 0 & 0 & 0 \\ 0 & -\frac{71\xi-22}{388} & -\frac{3\xi+10}{194} & \frac{3\xi+10}{388} & 0 \\ 0 & -\frac{3\xi+10}{194} & -\frac{18\xi-37}{388} & -\frac{3\xi+10}{194} & 0 \\ 0 & \frac{3\xi+10}{388} & -\frac{3\xi+10}{194} & -\frac{71\xi-22}{388} & 0 \\ 0 & 0 & 0 & 0 & -\frac{67\xi-3}{1552} \end{bmatrix};$$

$$Q = \begin{bmatrix} \frac{423\xi-45}{6208} & -\frac{199\xi-48}{2328} & -\frac{2\xi+39}{1552} & \frac{23\xi+12}{776} & -\frac{205\xi+69}{18624} \\ \frac{199\xi-48}{2328} & 0 & -\frac{7\xi-9}{194} & -\frac{23\xi+12}{291} & \frac{23\xi+12}{776} \\ \frac{2\xi+39}{1552} & \frac{7\xi-9}{194} & 0 & -\frac{7\xi-9}{194} & -\frac{2\xi+39}{1552} \\ -\frac{23\xi+12}{776} & \frac{23\xi+12}{291} & \frac{7\xi-9}{194} & 0 & -\frac{199\xi-48}{2328} \\ \frac{205\xi+69}{18624} & -\frac{23\xi+12}{776} & \frac{2\xi+39}{1552} & \frac{199\xi-48}{2328} & -\frac{423\xi-45}{6208} \end{bmatrix}.$$

The characteristic polynomial of the matrix P is

$$(194\lambda + 37\xi - 6)(1552\lambda + 67\xi - 3)^2$$
$$(37636\lambda^2 + 8342\xi\lambda - 6693\lambda + 288\xi^2 - 893\xi + 96) = 0$$

for which the roots are $\lambda = (-86\xi + 69 \pm \sqrt{2788\xi^2 + 2420\xi + 3225}/776$, $\lambda = -(67\xi - 3)/1552$, $\lambda = -(37\xi - 6)/194$. For values of $\xi < \frac{3}{67}$, all eigenvalues are positive, and the method is stable. The resulting matrix A^* can be written as

$$A^* = \begin{bmatrix} -\frac{423\xi-45}{268\xi-12} & \frac{398\xi-96}{201\xi-9} & \frac{2\xi+39}{67\xi-3} & -\frac{46\xi+24}{67\xi-3} & \frac{205\xi+69}{804\xi-36} \\ -\frac{104\xi-9}{222\xi-36} & \frac{3\xi+10}{74\xi-12} & \frac{7\xi-9}{37\xi-6} & \frac{83\xi+18}{222\xi-36} & -\frac{10\xi+1}{74\xi-12} \\ \frac{1}{12} & -\frac{2}{3} & 0 & \frac{2}{3} & -\frac{1}{12} \\ \frac{10\xi+1}{74\xi-12} & -\frac{83\xi+18}{222\xi-36} & -\frac{7\xi-9}{37\xi-6} & -\frac{3\xi+10}{74\xi-12} & \frac{104\xi-9}{222\xi-36} \\ -\frac{205\xi+69}{804\xi-36} & \frac{46\xi+24}{67\xi-3} & -\frac{2\xi+39}{67\xi-3} & -\frac{398\xi-96}{201\xi-9} & \frac{423\xi-45}{268\xi-12} \end{bmatrix}.$$

Note that for a value of $\xi = -\frac{10}{3}$ the resulting scheme is

$$P = \begin{bmatrix} \frac{7}{48} & 0 & 0 & 0 & 0 \\ 0 & \frac{2}{3} & 0 & 0 & 0 \\ 0 & 0 & \frac{1}{4} & 0 & 0 \\ 0 & 0 & 0 & \frac{2}{3} & 0 \\ 0 & 0 & 0 & 0 & \frac{7}{48} \end{bmatrix}; \quad Q = \begin{bmatrix} \frac{-15}{64} & \frac{11}{36} & \frac{-1}{48} & \frac{-1}{12} & \frac{19}{576} \\ \frac{-11}{36} & 0 & \frac{1}{6} & \frac{2}{9} & \frac{-1}{12} \\ \frac{1}{48} & \frac{-1}{6} & 0 & \frac{1}{6} & \frac{-1}{48} \\ \frac{1}{12} & \frac{-2}{9} & \frac{-1}{6} & 0 & \frac{11}{36} \\ \frac{-19}{576} & \frac{1}{12} & \frac{1}{48} & \frac{-11}{36} & \frac{15}{64} \end{bmatrix};$$

$$A^* = \begin{bmatrix} \frac{-45}{28} & \frac{44}{21} & \frac{-1}{7} & \frac{-4}{7} & \frac{19}{84} \\ \frac{-11}{24} & 0 & \frac{1}{4} & \frac{1}{3} & \frac{-1}{8} \\ \frac{1}{12} & \frac{-2}{3} & 0 & \frac{2}{3} & \frac{-1}{12} \\ \frac{1}{8} & \frac{-1}{3} & \frac{-1}{4} & 0 & \frac{11}{24} \\ \frac{-19}{84} & \frac{4}{7} & \frac{1}{7} & \frac{-44}{21} & \frac{45}{28} \end{bmatrix}.$$

Other third-order subelements exist for a uniform grid, but require a larger stencil. Their operation count is necessarily larger than those already presented and will not be pursued in this work.

Fourth Order

The optimal fourth-order schemes defined on five grid points produce a subelement A^* that can be decomposed into P and Q of the form

$$P = \begin{bmatrix} 1 & \frac{2}{3} & 0 & 0 & 0 \\ \frac{2}{3} & \frac{20}{3} & \frac{-10}{3} & \frac{4}{3} & 0 \\ 0 & \frac{-10}{3} & \frac{32}{3} & \frac{-10}{3} & 0 \\ 0 & \frac{4}{3} & \frac{-10}{3} & \frac{20}{3} & \frac{2}{3} \\ 0 & 0 & 0 & \frac{2}{3} & 1 \end{bmatrix}; \quad Q = \begin{bmatrix} \frac{-9}{4} & \frac{31}{9} & -2 & 1 & \frac{-7}{36} \\ \frac{-31}{9} & 0 & 6 & \frac{-32}{9} & 1 \\ 2 & -6 & 0 & 6 & -2 \\ -1 & \frac{32}{9} & -6 & 0 & \frac{31}{9} \\ \frac{7}{36} & -1 & 2 & \frac{-31}{9} & \frac{9}{4} \end{bmatrix};$$

$$A^* = \begin{bmatrix} \frac{-25}{12} & 4 & -3 & \frac{4}{3} & \frac{-1}{4} \\ \frac{-1}{4} & \frac{-5}{6} & \frac{3}{2} & \frac{-1}{2} & \frac{1}{12} \\ \frac{1}{12} & \frac{-2}{3} & 0 & \frac{2}{3} & \frac{-1}{12} \\ \frac{-1}{12} & \frac{1}{2} & \frac{-3}{2} & \frac{5}{6} & \frac{1}{4} \\ \frac{1}{4} & \frac{-4}{3} & 3 & -4 & \frac{25}{12} \end{bmatrix}.$$

Gershgorin's theorem can be used to prove that the matrix P is positive definite. The scheme satisfies all criteria of the summation-by-parts energy norm and is, therefore, stable for hyperbolic systems. Note that the resulting scheme is pentadiagonal in the matrix P and would require a banded solver in the cyclo-difference mode to invert. The operation count of just the $\hat{P}$ matrix inversion would be $5N$, which is not competitive with other explicit formulations. As the order of accuracy increases with optimal formulations, the bandwidth of the matrix P will also increase, which makes these schemes impractical.

A subelement of uniformly fourth-order schemes that is stable and explicit can be derived by considering six uniformly distributed discrete points. One additional degree of freedom from each point enables all of the constraints to be met. As with the third-order subelements, a matrix P that decouples is sought. Matrices P and Q that satisfy these constraints are

$$P = \begin{bmatrix} -\frac{1069\xi - 228785}{29668350} & 0 & 0 & 0 & 0 & 0 \\ 0 & -\frac{10993\xi - 800174}{7120404} & \frac{4819\xi - 234830}{2373468} & -\frac{4099\xi - 186200}{2373468} & \frac{4819\xi - 234830}{7120404} & 0 \\ 0 & \frac{4819\xi - 234830}{2373468} & \frac{9733\xi - 418388}{2373468} & \frac{2899\xi - 105150}{791156} & -\frac{4099\xi - 186200}{2373468} & 0 \\ 0 & -\frac{4099\xi - 186200}{2373468} & \frac{2899\xi - 105150}{791156} & -\frac{9733\xi - 418388}{2373468} & \frac{4819\xi - 234830}{2373468} & 0 \\ 0 & \frac{4819\xi - 234830}{7120404} & -\frac{4099\xi - 186200}{2373468} & \frac{4819\xi - 234830}{2373468} & -\frac{10993\xi - 800174}{7120404} & 0 \\ 0 & 0 & 0 & 0 & 0 & -\frac{1069\xi - 228785}{29668350} \end{bmatrix};$$

$$Q = \begin{bmatrix} \frac{3624\xi - 442560}{24723625} & -\frac{35723\xi - 2849575}{71204040} & \frac{29309\xi - 1476865}{35602020} & -\frac{3019\xi - 113255}{3955780} & \frac{13051\xi - 395255}{35602020} & -\frac{127303\xi - 3266195}{1780101000} \\ \frac{35723\xi - 2849575}{71204040} & 0 & -\frac{9689\xi - 448381}{7120404} & \frac{11713\xi - 255437}{7120404} & -\frac{5471\xi - 114043}{4746936} & \frac{13051\xi - 395255}{35602020} \\ -\frac{29309\xi - 1476865}{35602020} & \frac{9689\xi - 448381}{7120404} & 0 & -\frac{5053\xi - 102293}{3560202} & \frac{11713\xi - 255437}{7120404} & -\frac{3019\xi - 113255}{3955780} \\ \frac{3019\xi - 113255}{3955780} & -\frac{11713\xi - 255437}{7120404} & \frac{5053\xi - 102293}{3560202} & 0 & -\frac{9689\xi - 448381}{7120404} & \frac{29309\xi - 1476865}{35602020} \\ -\frac{13051\xi - 395255}{35602020} & \frac{5471\xi - 114043}{4746936} & -\frac{11713\xi - 255437}{7120404} & \frac{9689\xi - 448381}{7120404} & 0 & -\frac{35723\xi - 2849575}{71204040} \\ \frac{127303\xi - 3266195}{1780101000} & -\frac{13051\xi - 395255}{35602020} & \frac{3019\xi - 113255}{3955780} & -\frac{29309\xi - 1476865}{35602020} & \frac{35723\xi - 2849575}{71204040} & -\frac{3624\xi - 442560}{24723625} \end{bmatrix}.$$

The roots of the characteristic polynomial of the matrix P are

$$\lambda = -\frac{1069\xi - 228785}{29668350}, \quad \lambda = \frac{-1547\xi + 145693 \pm \sqrt{779521\xi^2 - 113722810\xi + 4192866925}}{2373468},$$

$$\lambda = \frac{-35551\xi + 1618259 \pm \sqrt{1105404637\xi^2 - 90611160610\xi + 1935582743125}}{7120404}$$

For values of $\xi < -498\sqrt{1153415558857} - 1018762117/13205747$ (a numerical value of about 36.64), all eigenvalues are positive, and the method is stable.

Fifth Order

Optimal subelements of fifth-order accuracy are not pursued in this work. Instead, a uniformly fifth-order accurate scheme defined on seven evenly spaced points is derived. The matrices P and Q are defined by

$$P = \begin{bmatrix} \frac{2345\xi + 2107188}{2606250528} & 0 & 0 & 0 & 0 & 0 & 0 \\ 0 & \frac{45759\xi + 8115844}{868750176} & -\frac{939\xi + 58732}{10342264} & \frac{2217\xi + 89104}{20684528} & -\frac{2217\xi + 89104}{31026792} & \frac{939\xi + 58732}{41369056} & 0 \\ 0 & -\frac{939\xi + 58732}{10342264} & \frac{181209\xi + 628420}{868750176} & -\frac{1317\xi - 41534}{5171132} & \frac{489\xi - 6587}{2585566} & -\frac{2217\xi + 89104}{31026792} & 0 \\ 0 & \frac{2217\xi + 89104}{20684528} & -\frac{1317\xi - 41534}{5171132} & \frac{220073\xi - 9105840}{651562632} & -\frac{1317\xi - 41534}{5171132} & \frac{2217\xi + 89104}{20684528} & 0 \\ 0 & -\frac{2217\xi + 89104}{31026792} & \frac{489\xi - 6587}{2585566} & -\frac{1317\xi - 41534}{5171132} & \frac{181209\xi + 628420}{868750176} & -\frac{939\xi + 58732}{10342264} & 0 \\ 0 & \frac{939\xi + 58732}{41369056} & -\frac{2217\xi + 89104}{31026792} & \frac{2217\xi + 89104}{20684528} & -\frac{939\xi + 58732}{10342264} & \frac{45759\xi + 8115844}{868750176} & 0 \\ 0 & 0 & 0 & 0 & 0 & 0 & \frac{2345\xi + 2107188}{2606250528} \end{bmatrix};$$

$$Q = \begin{bmatrix} -\frac{725\xi + 320700}{186160752} & \frac{134995\xi + 28687548}{8687501760} & -\frac{111545\xi + 7615668}{3475000704} & \frac{311185\xi + 1775124}{7818751584} \\ -\frac{134995\xi + 28687548}{8687501760} & 0 & \frac{86205\xi - 27052}{1737500352} & -\frac{8225\xi - 1176216}{108593772} \\ \frac{111545\xi + 7615668}{3475000704} & -\frac{86205\xi - 27052}{1737500352} & 0 & \frac{46445\xi - 14761644}{868750176} \\ -\frac{311185\xi + 1775124}{7818751584} & \frac{8225\xi - 1176216}{108593772} & -\frac{46445\xi - 14761644}{868750176} & 0 \\ \frac{24955\xi - 730068}{868750176} & -\frac{41265\xi - 7067356}{579166784} & \frac{272685\xi - 90860668}{3475000704} & -\frac{46445\xi - 14761644}{868750176} \\ -\frac{19495\xi - 1005492}{1737500352} & \frac{22155\xi - 2860208}{542968860} & -\frac{41265\xi - 7067356}{579166784} & \frac{8225\xi - 1176216}{108593772} \\ \frac{287735\xi - 19296756}{156375031680} & -\frac{19495\xi - 1005492}{1737500352} & \frac{24955\xi - 730068}{868750176} & -\frac{311185\xi + 1775124}{7818751584} \end{bmatrix} \cdots .$$

The remaining portion of the Q matrix can be obtained using skew symmetry and persymmetry arguments. The matrix P is positive definite for values of $\xi > 164.93 \ldots$ (determined numerically). This uniformly fifth-order scheme satisfies the summation-by-parts energy norm and can be used as the subelement for generating a cyclo-difference scheme. The resulting scheme will be explicit in nature because the matrix $\hat{P}$ can be inverted analytically.

This basic procedure can be used to generate schemes of arbitrarily high order, although none with an accuracy of greater the fifth order was generated in this work. For accuracies sixth-order and greater, the analytic values of the coefficient may exceed the precision of 64-bit arithmetic, and round-off error becomes important. In addition, the wisdom of approximating an arbitrary function on a uniform grid with extremely high order polynomials becomes questionable.

Finally, a comment about the extension of cyclo-difference schemes to multi-dimensions. Cyclo-difference schemes are extended to multi-dimensions in the same fashion as any conventional finite-difference scheme on a structured grid. The derivative operators in the coordinate directions j are formed sequentially as $P_j^{-1}Q_j$.

STABILITY OF THE CYCLO-DIFFERENCE SCHEMES

The summation-by-parts energy norm was used to develop the cyclo-difference schemes in a semidiscrete context. The theoretical CFL for various Runge–Kutta (R-K) schemes must still be determined. Because each point in a cyclo-difference scheme uses a different stencil, the use of Fourier techniques to obtain a CFL is not applicable. A numerically determined eigenvalue spectrum provides a practical means of obtaining the CFL of the various schemes.

For time asymptotic stability, all eigenvalues of the spatial discretization operator (scaled by Δt) must lie within the stability region of the time integration formula for all $\Delta t \leq \Delta t_{\max}$: the maximum stable Δt. This condition guarantees that the solution in time will remain bounded if the solution to the original governing equation is bounded. The determination of the CFL of a discretization is thus reduced to solving for $\Delta t_{\max}$ such that the resulting stability region of the time integration formula encompasses all spatial eigenvalues.

Figure 1 shows the eigenvalue spectrum of the cyclo-difference schemes as determined from a numerical eigenvalue determination. For each case, the number of grid points is 61; this number satisfies the grid constraints for all cyclo-difference schemes presented thus far. Note that the structure of the spectrum is not continuous, but it seems to cluster into specific portions of the complex plane as for conventional finite-difference techniques. (See Ref. [2].) In addition, this clustering becomes more pronounced as the order of accuracy increases.

Table I shows the CFLs of the various schemes determined from a numerical eigenvalue determination. In all cases, the

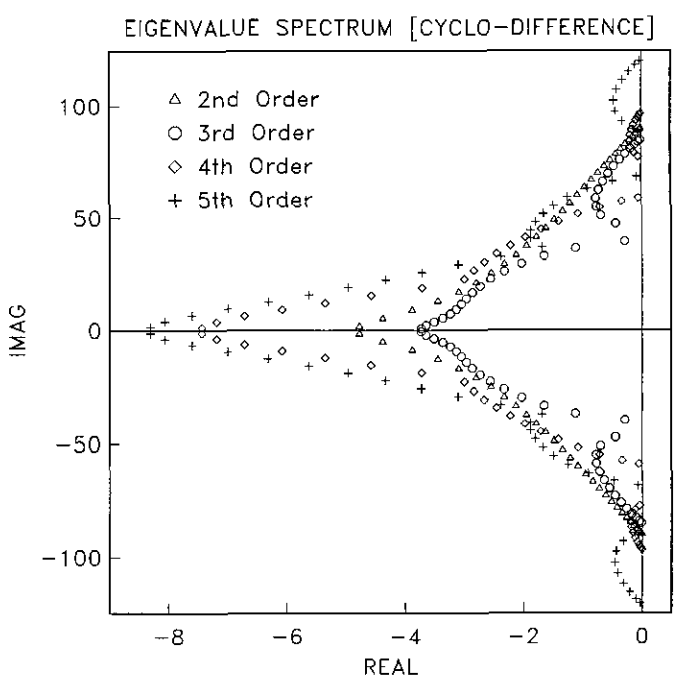

FIG. 1. Eigenvalue spectra for second- to fifth-order cyclo-difference schemes with 61 grid-points.

TABLE I

CFL of Cyclo-Difference Schemes Determined from Eigenvalue Determination

(R-K) order	CFL			
	Cyc23	Cyc35	Cyc46	Cyc57
2nd	Unstable	Unstable	Unstable	Unstable
3rd	1.16	1.23	1.08	0.87
4th	1.89	2.01	1.77	1.42

grid used contained 61 points. Very little sensitivity to grid density was observed between 31 and 61 grid points. The four algorithms used in the study were: (1) cyc23; (2) cyc35; (3) cyc46; (4) cyc57. The first number indicates the formal accuracy of the scheme; the last number is the number of grid points occupied by the subelement stencil. The cyclo-difference schemes are then generated by recursively appending the subelements. Note that each scheme can only run on a grid of $M(N-1)+1$ points, where N is the element size and M is the number of elements. Note that in each spatial operator, the fourth-order R-K is more efficient (in terms of CPU time, rather than storage) than the third-order R-K to advance the solution in time.

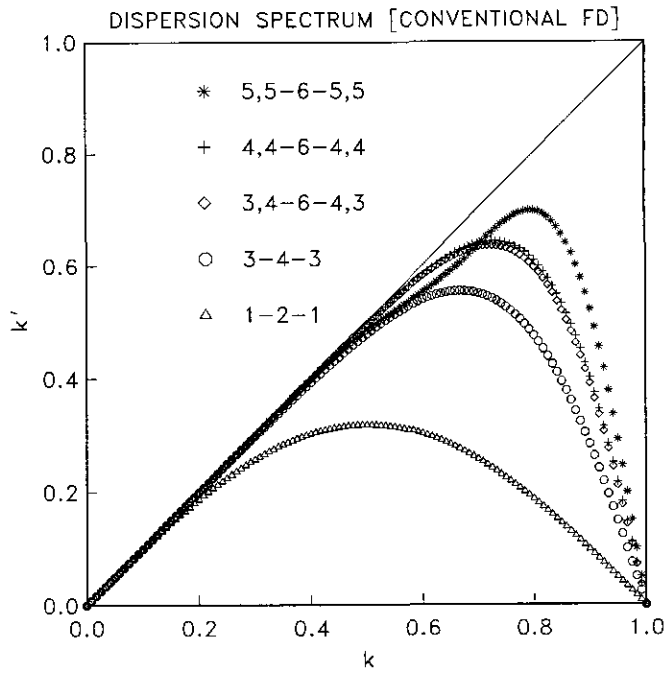

FIG. 2. Numerically determined dispersion spectrum of three conventional finite-difference schemes.

ACCURACY OF CYCLO-DIFFERENCE SCHEMES

Numerical Dispersion

The numerical dispersion of a conventional scheme can be quantified by comparing the Fourier image of the derivative operator with the image obtained by exact differentiation. For example, the Fourier image of the second-order central derivative operator $u_x = (u_{i+1} - u_{i-1})/2\delta x$ is $i \sin(k)$, while exact differentiation yields ik. Plotting the approximate result $k' = \sin k$ as a function of k shows in wave space the error committed by the numerical approximation for each Fourier mode. This analysis is valid on periodic domains, with identical stencils throughout, and provides a good approximation for the finite domain problem where identical stencils are not possible. For more detailed results, numerical techniques must be used for nonperiodic domains, with near-boundary stencils.

Figure 2 shows the numerical dispersion of three conventional schemes (with various boundary conditions) on a finite domain. The numerical schemes analyzed are: second-order central difference with first-order boundary conditions, (1-2-1); fourth-order compact with third-order boundary conditions, (3-4-3); and sixth-order compact with third-, fourth-, and fifth-order boundary conditions, (3, 4-6-4, 3), (4, 4-6-4, 4), and (5, 5-6-5, 5), respectively. (See Carpenter *et al.* [2] for specific details). To generate the discrete spectrum, a function composed of an individual Fourier mode was numerically differentiated. The resulting derivative function was Fourier analyzed, and the value of the k mode was assigned to be k'. In all cases, 241 grid points supporting 121 Fourier modes were used. The second- and fourth-order cases are indistinguishable on the plot from the corresponding periodic case. Note, however, the effects of the numerical boundary conditions on the sixth-order case.

The cyclo-difference schemes are not amenable to conventional Fourier dispersion analysis because a different stencil is used at each grid point. Figure 3 shows the numerical dispersion of the cyc35 scheme as a function of the independent parameter ξ. Only values of ξ for which the resulting scheme is numerically stable are studied. Note that the dispersion appears to be minimal near the value $\xi = -\frac{1}{4}$. The numerical error: $|k - k'|$, for $\xi = -\frac{1}{4}$, does not exceed 10^{-3} over the range $0 \leq k \leq \frac{1}{2}$. Figures 4 and 5 show the discrete dispersion spectrum of the cyc46 and cyc57 schemes, again plotted as a function of the independent parameter ξ. The erratic high wave number behavior of the cyclo schemes appears to increase with increasing accuracy. The exact cause of this behavior is unknown, but it could be related to the "Runge" phenomena seen in polynomial approximation theory on uniform grids [8]. Comparing Figs. 3 and 4, note that the cyc35 scheme has high wave number resolution which is comparable with the (3-4-3) scheme, making it a candidate for simulations which are not well grid-resolved. Conversely, the cyc57 scheme is not a good candidate for calculations which do not have eight grid points per wavelength.

Finally, we note that the inherent dissipation in the cyclo-

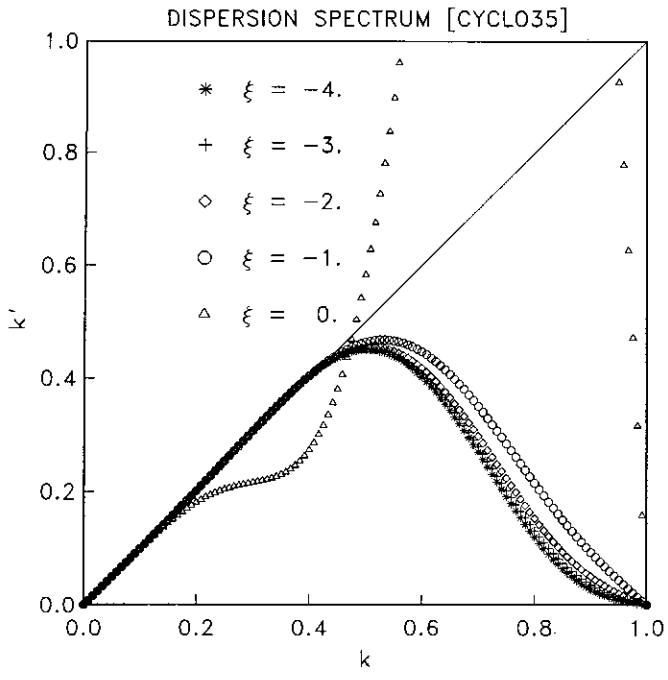

FIG. 3. Numerically determined dispersion spectrum of cyclo35 scheme, as a function of parameter ξ.

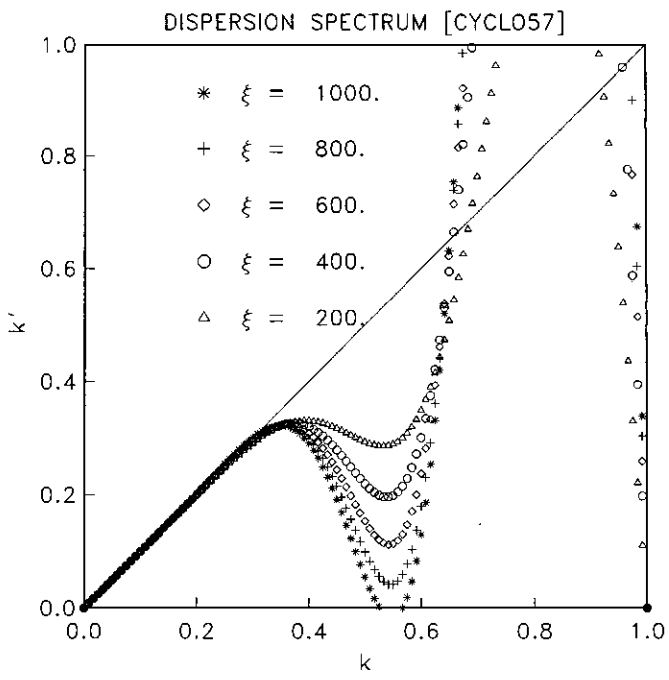

FIG. 5. Numerically determined dispersion spectrum of cyclo57 scheme, as a function of parameter ξ.

difference schemes comes from the temporal advancement scheme. Semi-discrete schemes which satisfy the summation-by-parts energy norm are neutrally dissipative in the P norm. (The eigenvalues are purely imaginary in the infinite and periodic cases). Runge–Kutta time advancement will introduce a modest amount of dissipation to the fully discrete equations.

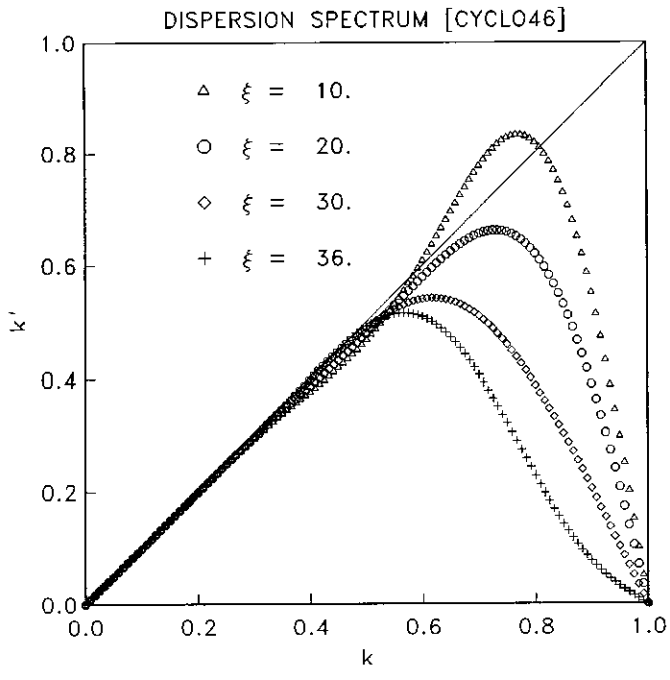

FIG. 4. Numerically determined dispersion spectrum of cyclo46 scheme, as a function of parameter ξ.

Time Dependent

Several test problems (both steady and unsteady) are used to establish the accuracy of the cyclo-difference schemes. Because Taylor series analysis was used in all cases to derive the schemes of a particular order, these schemes are expected to behave with at least the order of the local truncation error. Consider the method-of-lines approximation to the scalar wave equation

$$\frac{\partial U}{\partial t} + \frac{\partial U}{\partial x} = 0, \quad -1 \leq x \leq 1, t \geq 0, \tag{16}$$

$$U(t, -1) = \sin 2\pi(-1 - t); \quad U(0, x) = \sin 2\pi x, \quad -1 \leq x \leq 1, t \geq 0, \tag{17}$$

with the exact solutions given by

$$U(t, x) = \sin 2\pi(x - t), \quad -1 \leq x \leq 1, t \geq 0. \tag{18}$$

The spatial discretization is accomplished by the new cyclo-difference schemes of various order; time was advanced with a four-stage R-K time-advancement scheme (formal nonlinear accuracy of fourth order) with a CFL of 0.25 to a time level of 25. Further temporal refinement showed no improvement in the solution accuracy.

Uniform Mesh

We begin with a discretization on a uniform mesh. Table II shows the results from a grid-refinement study performed with each algorithm. Plotted is the log L_2 error as a function of the grid density, where $L_2 = \sqrt{\Sigma_j(\varepsilon_j)^2/N}$ with ε_j being the error at gridpoint j.

Once a scheme has achieved a certain minimum grid density it will exhibit an order property; by doubling the mesh, the error will decrease by a factor of 2^k, where k is the order of the scheme. The slopes for each scheme, as determined between grid densities of 31 (37 for cyc57) and 121 points, were −2.05, −4.05, −4.45, and −6.10, respectively.

Note that the apparent accuracy of some of the cyclo-difference schemes is higher than the predicted local truncation error. This result is more apparent in the schemes with an odd order, namely the cyc35 and the cyc57. The cyc46 does not obtain an accuracy that is significantly greater than the theoretical accuracy. Borrowing from the finite-element terminology, this increased convergence rate shall be referred to as "superconvergence."

Discontinuous Mesh

We noted earlier in the derivation of the underlying principles of cyclo-differencing that two subintervals of unequal spacing could be joined at an interface without destroying the accuracy or stability of the formulation. The discretization matrices $\hat{P}$ and $\hat{Q}$ were defined by

$$\hat{P} = \begin{bmatrix} \Delta_1 P & 0 \\ 0 & \Delta_2 P \end{bmatrix}; \quad \hat{Q} = \begin{bmatrix} Q & 0 \\ 0 & Q \end{bmatrix}.$$

TABLE II

Accuracy of New Cyclo-Difference Schemes as Function of Grid Density

	log L_2			
Grid	Cyc23	Cyc35	Cyc46	Cyc57
16			−1.347	
17		−0.7378		
19				−1.530
21	−1.662	−0.6959	−1.740	
25		−1.625		−2.059
29		−2.066		
31	−2.083		−2.276	−2.760
33		−2.218		
37				−3.273
41		−2.587	−2.722	
61	−2.710	−3.521	−3.736	−4.620
81		−3.914	−4.249	
91			−4.455	−5.678
101		−4.248	−4.638	
121	−3.316	−4.547	−4.956	−6.435

TABLE III(a)

Accuracy of cyc35-Difference Scheme for Discontinuous Mesh Spacing as a Function of Grid Density

	log L_2			
Grid	$\rho = 1$	$\rho = 3/2$	$\rho = 3$	$\rho = 5$
41	−2.587	−2.469	−1.864	−1.849
81	−3.914	−3.715	−3.197	−3.123
121	−4.547	−4.521	−3.974	−3.915
161	−5.046	−5.052	−4.559	−4.315

Table III(a) shows the results of a grid-refinement study for which the ratio of grid spacings between subintervals was not one ($\Delta 1/\Delta 2 \neq 1$). The model problem was that used in the previous test case (Eqs. (16) to (18)), and the spatial discretization was the cyc35 algorithm. Time advancement was as previously described. In each case, the spatial domain was divided into two regions, and one half of the total number of points was distributed uniformly throughout each domain. This gave rise to grid spacings $\Delta 1$ and $\Delta 2$ in each domain, respectively. Table III(a) shows the logarithm of the L_2 error for each discretization as a function of grid density, for a variety of spacing ratios $\rho = \Delta 1/\Delta 2$. In all cases, the finest concentration of mesh points occurred at the outflow boundary.

The magnitude of the error increases as the mesh discontinuity increases. This is because of the increased effective grid density that results from clustering the mesh points near the outflow boundary. The scheme still behaves with a fourth-order accuracy on this problem. Note that the slope of error decay for the $\rho = 5$ case is −3.96 between $N = 81$ and $N = 161$ and that the cyc35 scheme is still superconvergent.

Table III(b) shows a similar comparison with the other cyclo-difference algorithms; all cases were run with a grid ratio of $\rho = 5$. The slope of the error decay in the cyc57 scheme between points 61 and 121 is −5.82. The odd-order schemes, even in this discontinuous case, appear to be superconvergent.

TABLE III(b)

Accuracy of Cyclo-Difference Schemes for Discontinuous Mesh Spacing ($\rho = 5$) as a Function of Grid Density

	log L_2		
Grid	cyc35	cyc46	cyc57
41	−1.849	−2.317	
61			−3.251
81	−3.123	−3.279	
97			−4.449
121	−3.915	−3.983	−5.004
161	−4.315	−4.476	

Long-Time Calculations

Stencils that abruptly change, such as at a boundary interface, can cause spurious reflection at the interface [9]. The reflections behave according to the order property of the scheme, but they can be significant for moderate resolutions. The cyclo-difference methods are composed of numerous interface patches, each of which exhibits numerical reflection. It is reasonable to question whether the quality of the numerical solution is adversely affected by the refections over long integration times. To test this hypothesis, Eq. (16) is modified to the form

$$\frac{\partial U}{\partial t} + \frac{\partial U}{\partial x} = 0, \quad 0 \le x \le 480, t \ge 0, \tag{19}$$

$$U(t,0) = \frac{1}{2}\exp\left(-\ln 2\left(\frac{-t}{3}\right)^2\right);$$

$$U(0,x) = \frac{1}{2}\exp\left(-\ln 2\left(\frac{x}{3}\right)^2\right);$$

$$0 \le x \le 480, t \ge 0, \tag{20}$$

with the exact solutions given by

$$U(t,x) = \frac{1}{2}\exp\left(-\ln 2\left(\frac{x-t}{3}\right)^2\right); \quad 0 \le x\,480, t \ge 0. \tag{21}$$

Equations (19) through (20) were solved with the five-stage fourth-order 2N-storage Runge–Kutta scheme (RK54) [11]. The cyclo-difference operators used were the cyc35, cyc46, and cyc57 schemes, each which was run at two different values of the parameter ξ. The conventional spatial operators used were the fourth-order explicit, sixth-order compact spatial operators described in detail in Ref. [2], and the eighth-order compact operator described in reference [10]. The physical boundary condition was imposed by solving the differentiated boundary condition on the boundary with the RK54 procedure. This technique was shown by Carpenter *et al.* [12] to yield a fourth-order temporally accurate procedure. Specifically, the boundary condition is $d^3u(0,t)/dt^3 = g'''(t)$, where g is the physical boundary condition at the inflow plane.

Table IV shows the results of a refinement study comparing the cyclo-difference schemes with conventional finite-difference schemes. All schemes are compared on three grids and integrated to times of $T = 50$ and $T = 400$, respectively. The grids were chosen to be extremely coarse for this study: approximately three, six, and twelve grid points per width of the Gaussian initial condition. None of the numerical methods achieves its asymptotic accuracy on the coarsest grid. The intermediate grid provides a good indicator of the coarse resolution capabilities of the methods. The order property of each scheme can be determined by comparing the results from the intermediate and fine grids.

For long time integrations on coarse grids, the cyc35 scheme is as accurate as the conventional fourth-order finite-difference scheme, while the cyc46 scheme is marginally more accurate. Little improvement (in spite of the additional cost) is achieved with the cyc57 scheme on these extremely coarse grids. Adjusting the value of ξ produced little change in the accuracy of the solution. These results are in good agreement with the numerical dispersion analysis presented earlier for each scheme.

Steady State

The second test problem is the solution of the flow through a supersonic nozzle. The governing equations are the quasi-one-dimensional Euler equations. For this problem, an exact steady-state solution exists and can be used to compare the accuracy of the new cyclo-difference methods. The previously presented stability proof for the cyclo-difference scheme is only valid for the constant coefficient hyperbolic system. For the non-linear hyperbolic system there is no guarantee that stability will be achieved. Other numerical methods (without nonlinear stability proofs) are stable, however, and it is reasonable to

TABLE IV

Grid Refinement Study to $T = 50{,}400$ at CFL $= \frac{1}{10}$ with RK54 Time Advancement Scheme

		Cyclo 35		Cyclo 46		Cyclo 57			
$T = 50$	3-4-3	$\xi = \frac{-1}{4}$	$\xi = \frac{-10}{3}$	$\xi = 10$	$\xi = 30$	$\xi = 200$	$\xi = 1000$	5-6-5	7-8-7
241	−1.68	−1.65	−1.79	−1.71	−1.70	−1.82	−1.70	−1.57	−1.82
481	−2.44	−2.27	−2.11	−2.68	−2.60	−2.51	−2.44	−3.14	−3.05
961	−3.59	−3.42	−3.65	−3.62	−3.68	−3.75	−3.77	−5.20	−5.31
$T = 400$									
241	−1.43	−1.42	−1.42	−1.57	−1.58	−1.43	−1.43	−1.46	−1.81
481	−1.83	−1.75	−1.85	−2.07	−2.07	−1.89	−1.86	−3.06	−3.04
961	−2.71	−2.55	−3.03	−2.75	−2.81	−3.01	−2.89	−5.25	−5.31

Note. Plotted is the log L_2 error.

expect a robust numerical method to be stable. The governing equations are

$$\frac{\partial}{\partial t}(\rho A) + \frac{\partial}{\partial x}(\rho u A) = 0$$

$$\frac{\partial}{\partial t}(\rho u A) + \frac{\partial}{\partial x}[(\rho u^2 + p)A] = p\frac{\partial A}{\partial x} \tag{22}$$

$$\frac{\partial}{\partial t}(\rho e_t A) + \frac{\partial}{\partial x}[(\rho e_t + p)uA] = 0,$$

where $A = A(x)$ and $e_t = CvT + u^2/2$. Boundary conditions are imposed on the inflow plane for all three equations, and $A(x)$ is prescribed such that the flow remains supersonic throughout the entire domain. A four- and a five-stage R-K were used to time advance the solution to the steady state (machine precision of 10^{-13}). Residual smoothing was used to accelerate the convergence rate for the various schemes. Table V shows a comparison of the L_2 error that resulted from each of the four cyclo-difference schemes on various grids.

Note that by doubling the mesh, an error decay is produced with a slope of -2.00, -4.00, -4.29, and -6.00, respectively. These slopes agree with those obtained in the time-dependent case for simple linear advection. Again we see that the odd-ordered schemes are superconvergent.

Note that conventional second-order methods (as well as higher order central methods) with suitable boundary conditions will *not* converge to steady state for this and many other practical flow problems. The residual decreases only one order and then remains at this point indefinitely. This non-convergence is because the interior scheme is entirely dispersive; thus, the only dissipation in the spatial scheme comes from the boundary closure terms, which generally are not sufficient to damp the high frequency modes that can develop under non-linear circumstances. Higher order damping is explicitly added to these central-difference schemes to ensure that a steady-state solution can be found. The cyclo-difference schemes, by virtue of their cellular construction, can be used without additional damping. In practice, additional damping makes the scheme converge more rapidly, as expected.

TABLE V

Accuracy of Cyclo-Difference Schemes as Functions of Grid Density for One-Dimensional Nozzle Flow

	log L_2			
Grid	Cyc23	Cyc35	Cyc46	Cyc57
121	−4.122	−5.450	−6.410	−6.851
181	−4.474	−6.153	−7.178	−7.916
241	−4.723	−6.653	−7.703	−8.666

CONCLUSIONS

A new methodology referred to as "cyclo-differencing" is presented for defining stable high-order finite-difference schemes. They are similar to spectral element techniques of some arbitrary order, and are ideally suited for implementation on parallel machines. Unlike spectral element techniques, their existence does not rely on orthogonal polynomials or nonuniform grids. In principle, they can be devised of any order accuracy, although only schemes of sixth-order accuracy are pursued in this work. These new techniques rely on the summation-by-parts energy norm to establish formal stability for the scalar hyperbolic case. In addition, if the newly devised SAT method for imposing boundary conditions is used in conjunction with cyclo-differencing, then the resulting numerical method is formally stable for the hyperbolic system.

The cyclo-difference techniques are similar to central-difference techniques in that they are stable for right- or left-running waves, with appropriate placement of the physical boundary conditions. A decided advantage is that no numerical boundary conditions are required near the walls. Thus, high-order accuracy is assured throughout the entire domain. In addition, the cyclo-difference schemes can be patched together across arbitrary grid discontinuities and still retain their accuracy and stability.

A series of test problems are used to demonstrate the efficacy of the cyclo-difference methodology. The scalar advection equation is used to show the formal stability and accuracy of the second- to fifth-order cyclo-difference schemes. For the odd-order cyclo-difference schemes, the property of superconvergence is observed; specifically, these schemes converge at a rate one order higher than their theoretical accuracy on both uniform and discontinuous grids. A one-dimensional nozzle problem is used to demonstrate the robustness of the cyclo-difference techniques. Steady-state solutions, consistent with the order property of the spatial operator, are obtained without the addition of artificial damping to the formulations. Finally, the viscous Burgers equation is solved to demonstrate the use of the cyclo-difference technique for a nonlinear parabolic problem. Again, robust and accurate solutions are obtained in all cases.

APPENDIX A

Viscous Stability

Assume $P(\partial U/\partial x) = QU$, where P and Q are matrix operators and U is a vector of discrete values. The proof of stability for the cyclo-difference scheme developed in this work relies on very specific forms for the matrices P and Q. Specifically, $P = P^T$ and is positive definite; $Q = Q_{sm} + Q_{sk}$, where the only nonzero elements of Q_{sk} are $q_{0,0}$ and $q_{N,N}$, and $q_{0,0} = -q_{N,N} = -\alpha$; ($\alpha > 0$). This form of the derivative operator leads directly to a stable second-derivative operator. We begin

with a derivation of the continuous energy for the one-dimensional heat equation,

$$\frac{\partial U}{\partial t} = \alpha_d \frac{\partial^2 U}{\partial x^2}, \quad 0 \le x \le 1, t \ge 0,$$
$$U(0, t) = f(t); \quad U(1, t) = g(t) \tag{A.1}$$
$$U(x, 0) = \psi(x), \quad 0 \le x \le 1.$$

Note that boundary conditions based on the derivatives at $x = 0$ or $x = 1$ could have been imposed. An energy (defined as $\frac{1}{2}U^2$) is formed by multiplying Eq. (A.1) by U. Integration over the domain results in

$$E_t(t) = \int_0^1 \left[- \alpha_d U \frac{\partial^2(U)}{\partial x^2} \right] dx, \quad t \ge 0. \tag{A.2}$$

Integration by parts yields an expression of the form

$$E_t(t) = \alpha_d[U(1, t)U_x(1, t) - U(0, t)U_x(0, t)] - \int_0^1 \alpha_d \left(\frac{\partial U}{\partial x} \right)^2 dx, \quad t \ge 0. \tag{A.3}$$

The energy takes the form of a negative definite quantity plus the boundary data that involve the function and its derivatives at the boundaries.

If the second derivative in Eq. (A.1) is formed by twice operating with the first derivative operator, the semidiscrete form of Eq. (A.1) becomes

$$\frac{\partial U}{\partial t} = \alpha_d P^{-1} Q P^{-1} Q U, \quad t \ge 0. \tag{A.4}$$

If P is symmetric ($P = P^T$) and is positive definite, then P^{-1} is symmetric and positive definite. Similarly, because $Q = Q_{sym} + Q_{sk}$, we have $Q = 2Q_{sym} - Q^T$. By operating on Eq. (A.4) from the left by $U^T P$ and using the relationships between Q and Q^T, we obtain

$$E_t(t) = \alpha_d[2U^T Q_{sym}^T P^{-1} Q U - U^T Q^T P^{-1} Q U], \quad t \ge 0, \tag{A.5}$$

where E_t is the time rate of change of the discrete energy defined by $E(t) = U^T P U$. In defining $V = QU$, the second term on the right side of Eq. (A.5) is negative definite. Because of the sparseness of the matrix Q_{sym}^T, the first term reduces to α $[U(1)(\partial U/\partial x)(1) - U(0)(\partial U/\partial x)(0)]$ and Eq. (A.5) becomes

$$E_t(t) = \alpha_d \left[\left(U(1, t) \frac{\partial U}{\partial x}(1, t) - U(0, t) \frac{\partial U}{\partial x}(0, t) \right) - V^T P^{-1} V \right], \quad t \ge 0. \tag{A.6}$$

This expression for the discrete energy is identical to that obtained from the continuous case. Therefore, the discrete energy will behave like the continuous energy. However, note that this analysis is linear and does not guarantee stability in some problems of practical interest. For example, the same argument could have been used to demonstrate the stability of forming U_{2x} from two central-difference first derivatives. In fact, if U_{2x} is formed in this manner, no damping would result for the π mode in Fourier space, which ultimately would result in the growth of the odd–even mode in physical space for unresolved nonlinear calculations.

The cyclo-difference schemes do not appear to be as susceptible to the odd–even mode instability as the conventional central-difference schemes because a different stencil is used at each point. For example, consider the cyc35 scheme with the parameter $\xi = \frac{-1}{10}$. The resulting subelement $A^* = P^{-1}Q$ is

$$A^* = \begin{bmatrix} \frac{-9}{4} & \frac{14}{3} & -4 & 2 & \frac{-5}{12} \\ \frac{-1}{3} & \frac{-1}{2} & 1 & \frac{-1}{6} & 0 \\ \frac{1}{12} & \frac{-2}{3} & 0 & \frac{2}{3} & \frac{-1}{12} \\ 0 & \frac{1}{6} & -1 & \frac{1}{2} & \frac{1}{3} \\ \frac{5}{12} & -2 & 4 & \frac{-14}{3} & \frac{9}{4} \end{bmatrix}.$$

By forming the viscous derivative by the sequential operation of the first derivative operator $A_v = A^*A^*$, we obtain

$$A_v = \begin{bmatrix} 3 & -9 & 10 & -5 & 1 \\ 1 & -2 & 1 & 0 & 0 \\ 0 & 1 & -2 & 1 & 0 \\ 0 & 0 & 1 & -2 & 1 \\ 1 & -5 & 10 & -9 & 3 \end{bmatrix}.$$

The interior of this matrix is identical to the conventional second-order viscous derivative and is not susceptible to the odd–even mode. Truncation analysis shows the resulting viscous matrix to be uniformly second order. Numerical Fourier analysis on the viscous equations indicates that the "π" mode is modestly damped for practical grid densities.

To test the convergence rate of the viscous terms and the overall influence of the odd–even mode, the viscous Burgers equation is used. The equation is defined by $U_t + (0.5U^2)_x = \mu U_{xx}$, with boundary conditions $U(0, t) = U_0$ and $U(1, t) = 0$. The exact steady-state solution is given by

$$U(x) = U_0 \overline{U} \left[\frac{1 - \exp \overline{U} \operatorname{Re}(x - 1)}{1 + \exp \overline{U} \operatorname{Re}(x - 1)} \right],$$

TABLE A.I

Error from Various Cyclo-Difference Schemes on the Steady-State Burgers Equation

Grid	Fourth	Cyc35	Cyc46	Cyc57
51	−2.009		−3.547	
53		−3.405		
55				−2.975
101	−3.408	−4.663	−4.496	
103				−4.719
201	−4.879	−5.882	−6.233	
205				−6.807
401	−6.369	−7.087	−7.561	
403				−8.596

where $\mathrm{Re} = U_0/\mu$ and $\bar{U}$ is the solution of the equation

$$\frac{\bar{U}-1}{\bar{U}+1} = \exp(-\bar{U}\,\mathrm{Re})$$

and can be used to determine the error on a particular grid for this problem. Table A.I shows the results of a grid-refinement study on the viscous Burgers equation.

The $\log_{10}$ of the L_2 error are plotted as a function of the grid density. The convergence rate for the fourth, cyc35, cyc46, and cyc57 methods are 4.9, 4.0, 5.1, and 6.5, respectively, as determined between the 101 and 401 points. The viscosity was $\mu = 0.04$ which results in $\mathrm{Re} = 25$.

APPENDIX B

Periodic Stability

At least two cycles of the fundamental subelement are required to define a cyclo-difference scheme (which includes two boundaries and one patch). Schemes of greater grid density can be constructed by cyclically patching an arbitrary number of subelements together. The cyclo-difference schemes can be used, however, on a periodic domain. By construction, we will show how to generate a stable periodic scheme from any of the cyclo-difference schemes.

The periodic assumption is implemented by first requiring that grid points 1 and N are equivalent. Hence, the last row and column from the cyclo-difference scheme can be eliminated. (With this requirement, the minimum number of subelements required for the periodic case is three.) If points 1 and N are equivalent, then the stencils that require grid point N are "wrapped around" to point 1. Similarly, the stencil at point 1 is replaced with the interface stencil symmetrically relates points on either side of grid point 1. The resulting cyclo-difference stencil is now periodic, and each subelement is indistinguishable in terms of position. Unlike conventional central-difference schemes, the resulting stencil is not skew symmetric. The eigenvalues of the stencil are all on the imaginary axis because $A_p = P_p^{-1}Q_p$, and Q_p is entirely skew symmetric.

The periodic versions of the cyc23 and cyc35 schemes are presented to illustrate this procedure. The periodic cyc23 scheme with three subelements (seven points) and truncated to six points, can be written as

$$A_p = \begin{bmatrix} 0 & 1 & \frac{-1}{4} & 0 & \frac{1}{4} & -1 \\ \frac{-1}{2} & 0 & \frac{1}{2} & 0 & 0 & 0 \\ \frac{1}{4} & -1 & 0 & 1 & \frac{-1}{4} & 0 \\ 0 & 0 & \frac{-1}{2} & 0 & \frac{1}{2} & 0 \\ \frac{-1}{4} & 0 & \frac{1}{4} & -1 & 0 & 1 \\ \frac{1}{2} & 0 & 0 & 0 & \frac{-1}{2} & 0 \end{bmatrix}.$$

The matrix $A_p = P_p^{-1}Q_p$, where P is the diagonal matrix characterized by $[\frac{1}{2}, 1, \frac{1}{2}, 1, \frac{1}{2}, 1]$ on the main diagonal; Q_p is entirely skew symmetric. By definition, we know that a skew symmetric matrix has eigenvalues on the imaginary axis. The semidiscrete energy of the system defined by $U^T P_p U$ will be unchanged for all time with this discretization.

A comparison of the eigenvalues for this discretization with those of the conventional second-order periodic central-difference stencil on six points is interesting. The characteristic polynomial for the matrix A_p is $\lambda^2(16\lambda^4 + 51\lambda^2 + 36) = 0$, which results in the eigenvalues $\lambda = 0$ and $\lambda = \pm\sqrt{3/32}\sqrt{17 \pm \sqrt{33}i}$ for which the maximum eigenvalue is ± 1.46024. The conventional periodic second-order scheme produces a characteristic polynomial $\lambda^2(4\lambda^2 + 3)^2 = 0$ for which the maximum eigenvalue is $\sqrt{3/4}i$. These eigenvalues are distinctly different; the effective CFL will be smaller for the cyc23 than for the conventional second-order scheme.

For simplicity, the diagonal form of the cyc35 scheme ($\xi = -\frac{10}{3}$) will be used to illustrate the periodic form of the operator. The subelement A_5 takes the form

$$A_5 = \begin{bmatrix} -\frac{45}{28} & \frac{44}{21} & \frac{-1}{7} & \frac{-4}{7} & \frac{19}{84} \\ -\frac{11}{24} & 0 & \frac{1}{4} & \frac{1}{3} & \frac{-1}{8} \\ \frac{1}{12} & \frac{-2}{3} & 0 & \frac{2}{3} & \frac{-1}{12} \\ \frac{1}{8} & \frac{-1}{3} & \frac{-1}{4} & 0 & \frac{11}{24} \\ -\frac{19}{84} & \frac{4}{7} & \frac{1}{7} & -\frac{44}{21} & \frac{45}{28} \end{bmatrix}.$$

Three subelements are used, and the resulting scheme is reduced by one row and column, which yields a matrix A_p of the form

$$A_p = \begin{bmatrix}
0 & \frac{22}{21} & \frac{-1}{14} & \frac{-2}{7} & \frac{19}{168} & 0 & 0 & 0 & -\frac{19}{168} & \frac{2}{7} & \frac{1}{14} & -\frac{22}{21} \\
-\frac{11}{24} & 0 & \frac{1}{4} & \frac{1}{3} & \frac{-1}{8} & 0 & 0 & 0 & 0 & 0 & 0 & 0 \\
\frac{1}{12} & \frac{-2}{3} & 0 & \frac{2}{3} & \frac{-1}{12} & 0 & 0 & 0 & 0 & 0 & 0 & 0 \\
\frac{1}{8} & \frac{-1}{3} & \frac{-1}{4} & 0 & \frac{11}{24} & 0 & 0 & 0 & 0 & 0 & 0 & 0 \\
-\frac{19}{168} & \frac{2}{7} & \frac{1}{14} & -\frac{22}{21} & 0 & \frac{22}{21} & \frac{-1}{14} & \frac{-2}{7} & \frac{19}{168} & 0 & 0 & 0 \\
0 & 0 & 0 & 0 & -\frac{11}{24} & 0 & \frac{1}{4} & \frac{1}{3} & \frac{-1}{8} & 0 & 0 & 0 \\
0 & 0 & 0 & 0 & \frac{1}{12} & \frac{-2}{3} & 0 & \frac{2}{3} & \frac{-1}{12} & 0 & 0 & 0 \\
0 & 0 & 0 & 0 & \frac{1}{8} & \frac{-1}{3} & \frac{-1}{4} & 0 & \frac{11}{24} & 0 & 0 & 0 \\
\frac{19}{168} & 0 & 0 & 0 & -\frac{19}{168} & \frac{2}{7} & \frac{1}{14} & -\frac{22}{21} & 0 & \frac{22}{21} & \frac{-1}{14} & \frac{-2}{7} \\
\frac{-1}{8} & 0 & 0 & 0 & 0 & 0 & 0 & 0 & -\frac{11}{24} & 0 & \frac{1}{4} & \frac{1}{3} \\
\frac{-1}{12} & 0 & 0 & 0 & 0 & 0 & 0 & 0 & \frac{1}{12} & \frac{-2}{3} & 0 & \frac{2}{3} \\
\frac{11}{24} & 0 & 0 & 0 & 0 & 0 & 0 & 0 & \frac{1}{8} & \frac{-1}{3} & \frac{-1}{4} & 0
\end{bmatrix}.$$

The matrix $A_p = P_p^{-1}Q_p$, where P is the diagonal matrix characterized by $[2, \frac{32}{7}, \frac{12}{7}, \frac{32}{7}, 2, \frac{32}{7}, \frac{12}{7}, \frac{32}{7}, 2, \frac{32}{7}, \frac{12}{7}, \frac{32}{7}]$ on the main diagonal and Q_p is entirely skew symmetric. The semidiscrete energy of the system defined by $U^T P_p U$ will be unchanged for all time with this discretization and is, therefore, stable when advanced with a stable time-advancement scheme. The characteristic polynomial for the matrix A_p is $x^2\,(x^2 + 2)\,(9408x^8 + 23545x^6 + 18219x^4 + 4302x^2 + 243) = 0$. The roots of this polynomial are strictly imaginary and are bounded by the points $\pm\sqrt{2}i$. Because the cyc35 scheme exhibits superconvergence properties, it can be compared with the conventional periodic fourth-order central difference expression defined on 12 grid points. The characteristic polynomial for the central difference case is $x^2(9x^2 + 16)(16x^2 + 27)(48x^2 + 49)(20736x^4 + 19296x^2 + 3721) = 0$. All roots are imaginary and are bounded by the points $\pm\frac{4}{3}i$. Again, note that the cyc35 scheme has a slightly more restrictive CFL than the conventional central-difference method on 12 points.

REFERENCES

1. B. Gustafsson, *Math. Comput.* **29,** 130, 396 (1975).
2. M. H. Carpenter, D. Gottlieb, and S. Abarbanel, *J. Comput. Phys.* **108,** No. 2 (1993).
3. H.-O. Kreiss and G. Scherer, "Finite Element and Finite Difference Methods for Hyperbolic Partial Differential Equations," in *Mathematical Aspects of Finite Elements in Partial Differential Equations* (Academic Press, New York, 1974).
4. B. Strand, *J. Comput. Phys.* **110,** No. 1 (1994).
5. M. H. Carpenter, D. Gottlieb, and S. Abarbanel, *J. Comput. Phys.* **111,** No. 2 (1994).
6. G. E. Karniadakis and S. A. Orszag, *SuperComputing in Engineering Analysis*, edited by H. Adeli.
7. M. G. Macaraeg and C. L. Streett, *Appl. Numer. Math.* **2,** No. 95 (1986).
8. G. Dahlquist, A. Bjorck, and N. Anderson, *Numerical Methods* (Prentice–Hall, Englewood Cliffs, NJ, 1974).
9. L. N. Trefethen, *Math. Comput.* **45,** No. 172 (1985).
10. C. A. Kennedy and M. H. Carpenter, *Appl. Numer. Math.* **14,** (1994).
11. M. H. Carpenter and C. A. Kennedy, NASA-TM-109111, April 1994; *SIAM J. Sci. Comput.*, submitted.
12. M. H. Carpenter, D. Gottlieb, S. Abarbanel, and W.-S. Don, NASA-CR-191561, ICASE Report No. 93-83, Dec. 1993; *SIAM J. Sci. Comput.*, to appear.